JOURNAL OF ENVIRONMENTAL SCIENCES 124 (2023) 440–450

Available online at www.sciencedirect.com

ScienceDirect

www.elsevier.com/locate/jes

JES JOURNAL OF ENVIRONMENTAL SCIENCES

www.jesc.ac.cn

Variability of turbulence dispersion characteristics during heavy haze process: A case study in Beijing

Lei Liu[1], *Yu Shi*[1], *Zhe Zhang*[1], *Fei Hu*[1,2,*]

[1] *LAPC, Institute of Atmospheric Physics, Chinese Academy of Sciences, Beijing 100029, China*
[2] *University of Chinese Academy of Sciences, Beijing 100049, China*

ARTICLE INFO

Article history:
Received 2 August 2021
Revised 16 September 2021
Accepted 30 October 2021
Available online 14 February 2022

Keywords:
Heavy haze
Turbulence dispersion
Local similarity
Lagrangian model

ABSTRACT

The turbulent standard deviations and the turbulent third-order and fourth-order moments are the key turbulence dispersion parameters in Lagrangian dispersion models. However, the characteristics of these parameters under heavy haze conditions in urban areas have not been fully investigated, and the commonly used similarity relations of these parameters in models were based on observations in highly flat and sparsely populated areas. In this paper, the vertical profiles of these parameters and their local similarity relations under heavy haze conditions in the wintertime of Beijing have been analyzed by using data collected at a 325-m meteorological tower. The heavy haze process has been divided into three stages: transport stage (TS), cumulative stage (CS), and dispersion stage (DS). Results show that the turbulent dispersion parameters behave differently during three stages. In the TS and DS, the maxima appear in the profiles of the turbulent standard deviations above the urban canopy; in the CS, the turbulent standard deviation are almost constant with height. The analysis of the third and fourth order moments shows that the wind velocities above the urban canopy in the TS deviate from the Gaussian distribution more significantly than those in the CS and DS. The local similarity relations of the turbulent dispersion parameters in the TS, especially for the longitudinal wind components, are normally different from those in the CS and DS. Thus, different from the common assumptions in Lagrangian models, the turbulence dispersion in horizontal directions is anisotropic and should be parameterized by multiple similarity relations under heavy haze conditions.

Introduction

The heavy haze pollution commonly occurs in the wintertime of Beijing and causes serious health problems. The boundary-layer meteorological factors that are not conducive to the pollutant dispersion are generally considered to be important causes of the wintertime heavy haze pollution. These factors include temperature inversion, high humidity, calm wind, and weak turbulence, and so on (Zhong et al., 2017a,b; Wang et al., 2019; Zhang et al., 2019; Bei et al., 2020). Among these meteorological factors, turbulence plays a two-sided role. On the one hand, weak turbulence is not conducive to disperse pollutants generated near the surface (Miao et al., 2015). On the other hand, strong turbulence can transfer the pollutants that are generated or transferred from a long distance in the upper air downward to the surface, which also causes heavy pollution near the surface (Salmond and McKendry, 2005; Li et al., 2017; Hong et al., 2021).

* Corresponding author.
E-mail: hufei@mail.iap.ac.cn (F. Hu).

https://doi.org/10.1016/j.jes.2021.10.034
1001-0742/

Except the Eulerian models, the Lagrangian model is also widely used in the analysis of heavy haze process, including analyzing aerosol trajectory, tracking pollutant source, and forecasting $PM_{2.5}$ concentration (Du et al., 2019; Bei et al., 2020; Guo et al., 2020). In the Lagrangian model, the turbulence dispersion is described by the Langevine equation (Thomson, 1987). The coefficients of the Langevine equation, that is turbulence dispersion parameters, are parameterized by similarity relations found in field observations. Nevertheless, the commonly used similarity relations are based on observations in highly flat and sparsely populated areas without heavy haze pollution. For example, the similarity relations in the FLEXPART model are based on the 1973 Minnesota experiment, which was conducted in a highly flat and sparsely populated grassed area (Panofsky et al., 1977).

The similarity relations based on observations in highly flat and sparsely populated areas can not represent turbulence dispersion in rough and densely populated urban areas. Firstly, the underlying theory of similarity relations in flat areas, that is the Monin-Obukhov similarity theory, is not generally true in urban areas. The rough sublayer where turbulence is strongly affected by buildings is usually thick, especially in the megacity, and the constant flux layer is hardly observed (Roth, 2000). Therefore, the local similarity theory is recommended to analyze urban observations, where local friction velocity and local heat flux replace their surface values in the Monin-Obukhov similarity theory (Al-Jiboori et al., 2002; Wood et al., 2010). Secondly, a typical heavy haze process in wintertime of Beijing is divided into three stages, according to the boundary-layer meteorological characteristics (Zhong et al., 2017a,b). The meteorological characteristics in each stage are significantly different from others. Turbulence dispersion characteristics and the similarity relations, which are affected by the boundary-layer meteorological characteristics, would be changed during different stages; however, this has not been fully investigated.

In this study, we mainly investigate the local similarity relations of turbulence dispersion parameters under heavy haze conditions in wintertime of Beijing. The heavy haze process is divided into three stages, and the boundary-layer meteorological characteristics in each stage are discussed in Section 2.1. The vertical profiles and the local similarity relations of turbulence dispersion parameters, including turbulent standard deviations and turbulent third and fourth order moments are discussed in Section 2.2-2.4.

1. Data and methods

The meteorological data were collected on a 325-m meteorological tower in the downtown of Beijing, China (39.97 °N, 116.37 °E). Within 5 kilometers of the tower, there are buildings with a height of about 10-60 m. About 200 m away to the west of the tower, there are a north-south highway bridge and a ring road. About 150 m away to the north of the tower, there is an east-west busy road. The wind speed and wind direction (010C cup anemometers and 020C wind vanes, Metone, USA), air temperature and humidity (HC2S3, Rotronic, Switzerland), were collected at 15 levels (8-, 15-, 32-, 47-, 65-, 80-, 100-, 120-, 140-, 160-, 180-, 200-, 240-, 280-, and 320-m) every minute. The 10-Hz turbulent wind velocity and temperature, were collected by ultrasonic anemometers (Windmaster Pro, Gill, UK) deployed at 7 levels (8-, 16-, 47-, 80-, 140-, 200-, and 280-m). More details about the meteorological tower are referred to literatures (Wang et al., 2019; Shi and Hu, 2020; Liu et al., 2021).

The hourly PM2.5 data collected from the environment monitoring station at the Olympic Sports Center are used in this paper (http://106.37.208.233:20035/). This station is about 2.5 km away to the northeast of the 325-m meteorological tower. The data collected on the heavy haze days from Nov 30 to Dec 4, in 2017 are analyzed. During these days, the maximum daily averaged $PM_{2.5}$ mass concentration is 152 $\mu g/m^3$, which is much greater than the limit of Ambient Air Quality Standards in China (75 $\mu g/m^3$ in GB 3095-2012).

The quality control methods, which are proposed by Vickers and Mahrt (1997) and include spikes, dropouts, data with discontinuities, data violating absolute limits, data with the amplitude resolution problem, data with unphysical high-order moments, are used to find problematic data. The time series seriously contaminated by the problematic data are removed in the analysis. The time series seriously contaminated by high-frequency white noises are also removed. After quality control and noise detection, about 2.52% 80-m, 2.86% 140-m, 3.30% 200-m, and 3.13% 280-m turbulence data are removed in the following analysis.

The instrument reference frame is transformed to the streamline reference frame by the double rotation (Kaimal and Finnigan, 1994). The average time in this paper is settled to 30 min as in many literatures (Wood et al., 2010; Yusup and Anis, 2016; Pegahfar and Zawarreza, 2017; Ren et al., 2019; Shi and Hu, 2020). To reduce the effect of urban canopy, only data above 80 m are used to analyze the similarity relations of turbulent dispersion parameters.

2. Results

2.1. *Meteorological characteristics under heavy haze conditions*

The hourly $PM_{2.5}$ mass concentrations and the corresponding meteorological fields under heavy haze conditions from Nov 30 to Dec 4 in 2017 are shown in Fig. 1. This process has been extensively analyzed in Liu et al. (2021). Here we only list the main characteristics briefly.

The time series of $PM_{2.5}$ mass concentration shows a typical ramp structure (Shi and Hu, 2020), where the concentration increases slowly and drops down more quickly (see Fig. 1a). According to Zhong et al. (2017a, b), the ramp structure is generally divided into three stages: transport stage (TS), cumulative stage (CS), and dispersion stage (DS).

(i) *Transport Stage (TS)*. During this stage (from 16:00 Nov 30 to 23:00 Dec 2), the wind directions are typically southwest (Fig. 1b). The pollutants generated from industrial cities in the southwest direction are then transported to Beijing (Li et al., 2017; Zhong et al., 2017a, b; Zhang et al., 2019), and the $PM_{2.5}$ mass concentration begins to grow (Fig.1a). Because the southwest wind is warm and wet, the temperature (Fig. 1c) and humidity (Fig. 1d) also

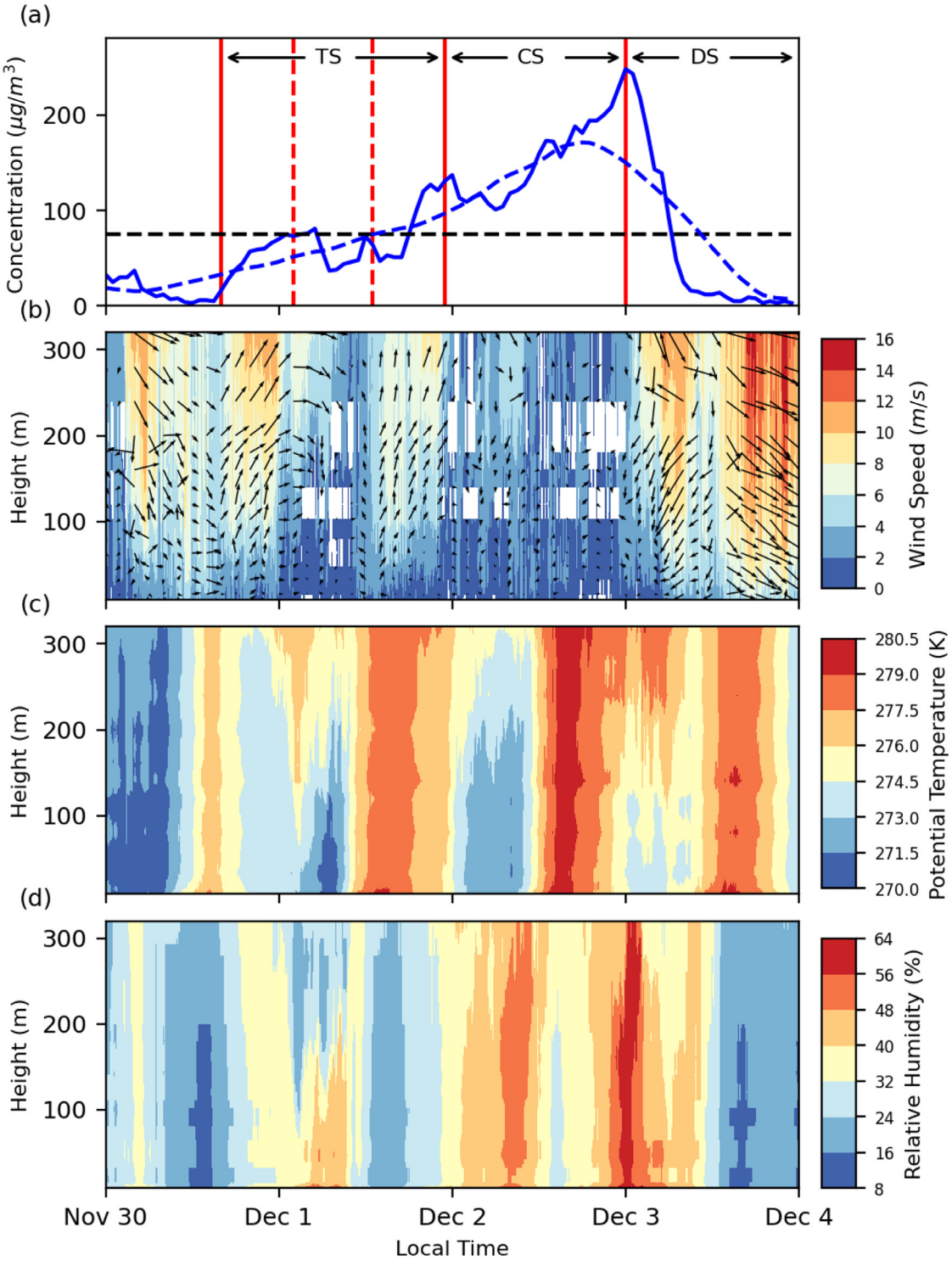

Fig. 1 – (a) The hourly PM2.5 mass concentration measured at the Olympic Sports Center Station from Nov 30 to Dec 4 in 2017. The transport stage (TS), the cumulative stage (CS), and the dispersion stage (DS) have been marked by red lines. The data fall in the period between red broken lines are removed in the TS analysis. The wind speed and direction, potential temperature, and relative humidity are shown in (b), (c), and (d) respectively

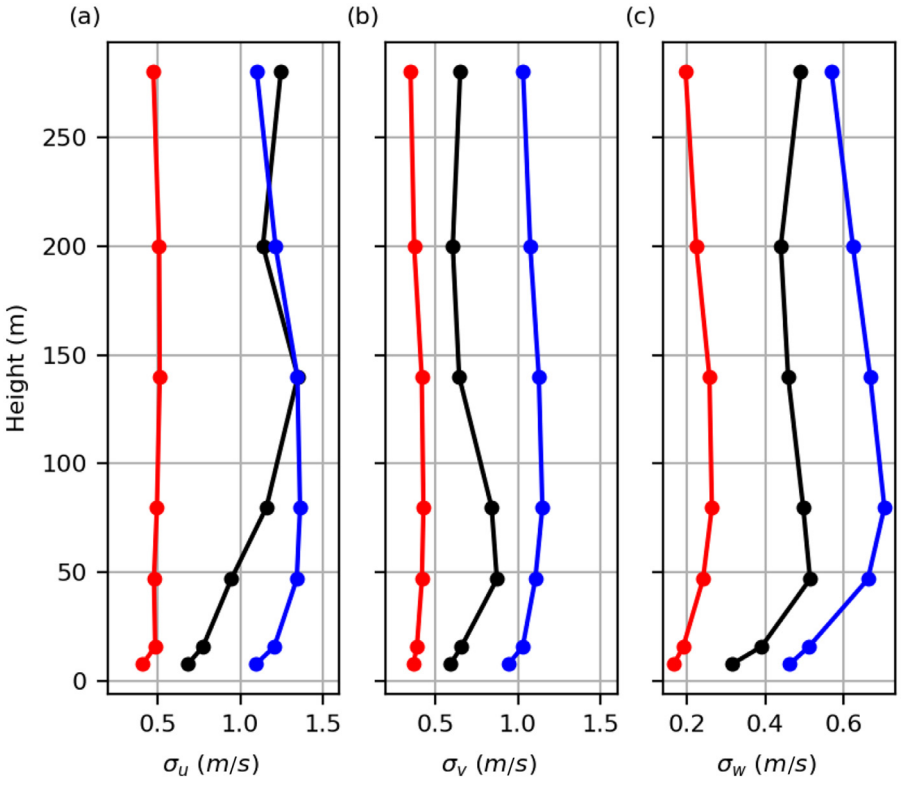

Fig. 2 – Profiles of turbulent standard deviations for (a) longitudinal, (b) transversal, and (c) vertical wind velocities in the TS (black), the CS (red) and the DS (blue).

increase significantly during the TS. From 2:00 to 13:00 on Dec 1 (between broken lines in Fig. 1a), the dominant wind direction changes from southwest to northwest. The northwest wind is cleaner, but the wind speeds are too small to disperse pollutants. After a slight decrease, the $PM_{2.5}$ mass concentration continues to increase until the dominant wind direction changes to southwest. The data with the northwest direction are removed in the TS analysis.

(ii) *Cumulative Stage (CS)*. During this stage (from 23:00 Dec 1 to 0:00 Dec 3), the wind speeds are generally small (Fig. 1b). The strong temperature inversion also occurs from the early morning of Dec 2 and lasts until about 11:00 on this day (Fig. 1c). The synergy of low wind speed and strong temperature inversion leads to the rapid accumulation of pollutants. The hourly $PM_{2.5}$ mass concentration increases by about 100 $\mu g/m^3$ in 12 hours.

(iii) *Dispersion Stage (DS)*. During this stage (from 0:00 Dec 3 to 23:00 Dec 3), strong wind from northern mountains disperses pollutants. The hourly $PM_{2.5}$ mass concentration drops dramatically from 248 $\mu g/m^3$to 25 $\mu g/m^3$ in 8 hours. The north wind is dry and cold. The temperature and humidity are observed to decrease in this stage (Figs. 1c and d).

2.2. *Turbulent standard deviation*

The turbulent standard deviations of wind velocities are key parameters in the study of turbulence dispersion. For example, the mean spread rate of particles is directly related to turbulent velocity standard deviations for stationary and homogeneous turbulence (Thomson, 1987). In the Lagrangian models, turbulence dispersion is described by the Langevine equation with turbulence velocity standard deviations as the main parameters.

The profiles of turbulent standard deviations for lateral, transverse, and vertical velocities (denoted by σ_u, σ_v, and σ_w respectively) during the transport stage (TS), the cumulative stage (CS), and the dispersion stage (DS) are shown in Fig. 2. Normally, it is found that $\sigma_u > \sigma_v > \sigma_w$, no matter in what stage. This is in contradiction with the common assumption of the similarity relations in the Lagrangian models, where σ_u is assumed to equal to σ_v (Stohl et al., 2005). In different stages, the variations of the turbulent standard deviations are different. First, the turbulent standard deviations in the DS are generally larger than those in the TS, and the latter is generally larger than those in the CS. This could be related to the wind speeds. The dominant wind speeds in the DS are generally larger than those in the TS, and the latter are generally larger than those in the CS (see Fig. 1b). Second, pronounced maxima are observed in the profiles of turbulent standard deviations in the TS and DS. The maxima could be related to strong turbulence generated by large wind shears at the urban canopy top. The wind shear is formed when air flows over buildings. Many filed observations and wind-tunnel experiments have found that turbulent kinetic energy over urban areas indeed shows a maximum at the urban canopy top (Kastner-Klein and Rotach, 2004; Christen et al., 2009;

Giometto et al., 2016). In the CS, the drag effect would not be significant with small wind speeds, and the profiles are nearly constant.

According to the local similarity theory, the dimensionless turbulent standard deviations σ_i/u_l ($i = u, v,$ or w) are functions of z/Λ, that is,

$$\frac{\sigma_i}{u_l} = f\left(\frac{z}{\Lambda}\right), \tag{1}$$

where, z is the observation height, u_l is the local friction velocity, Λ is the local Obukhov length, and f is the local similarity function. The scales u_l and Λ are calculated at the observation height. The local Obukhov length is

$$\Lambda = -\frac{\bar{\theta}_v u_l^3}{kg\left(\overline{w'\theta_v'}\right)}$$

where $\bar{\theta}_v$ is the virtual potential temperature, $\overline{w'\theta_v'}$ is the heat flux, k is the von Karman constant, and g is the acceleration due to gravity. The virtual potential temperature is estimated by (Stull, 1988)

$$\bar{\theta}_v = T_v + (g/C_p)z$$

where, T_v is the virtual temperature measured by the ultrasonic anemometers and C_p is the specific heat of dry air at constant pressure. The thermal stability can depress turbulence when the heat is transported downward ($\overline{w'\theta_v'} < 0$); The thermal instability can maintain turbulence when the heat is transported upward ($\overline{w'\theta_v'} > 0$). Thus, the sign of z/Λ can be used to indicate the local static stability: negative means unstable and positive means stable (Stull, 1988).

The local similarity function $f(z/\Lambda)$ could be fitted by

$$f\left(\frac{z}{\Lambda}\right) = \left(a + b\frac{z}{|\Lambda|}\right)^c, \tag{2}$$

where, a, b, and c are fitting parameters (Al-Jiboori et al., 2002; Wood et al., 2010; Fortuniak et al., 2013). At the neutral condition, $z/\Lambda = 0$. Thus, the dimensionless turbulent standard deviations equal to a constant of a. At the highly unstable conditions,

$$f\left(\frac{z}{\Lambda}\right) \sim \left(-\frac{z}{\Lambda}\right)^c$$

According to the assumption of local free convection (Garratt, 1992), the Reynold stress becomes insignificant and u_l ceases to be a relevant scale in similarity relations. In order to eliminate u_l on both sides of Eq. (1), one can deduce that the free convention exponent $c = 1/3$.

The local similarity functions of turbulent standard deviations are shown in Fig. 3. It is found that the similarity functions in the TS are generally different from those in the CS and DS, especially for σ_u and σ_w. The values of σ_u/u_l during TS is large than those in the CS and DS. At highly stable or unstable conditions, the values of σ_w/u_l during TS increases more quickly than those in the CS and DS The nearly neutral values of σ_u/u_l, σ_v/u_l, and σ_w/u_l in literatures are normally in the ranges of 1.75-3.23, 1.60-3.42, and 1.10-2.38 respectively (see Table 1). Most values in the present study fall in these ranges (see Table 2). The assumption of local free convection that the free convection exponent equals 1/3 is controversial in literatures (see Table 1). The results in the present study show that the turbulent standard deviations under heavy haze conditions generally deviate from this assumption (see Fig. 3 and Table 2).

2.3. *Turbulent third and fourth order moments*

In the convective boundary layer, the non-zero skewness (the dimensionless third-order moment) of turbulent vertical velocity plays a vital role in the vertical dispersion of particles (Luhar et al., 2000). The latest version of the FLEXPART model has implemented the bi-Gaussian model with a non-zero skewness to simulate dispersion near sources in the convective boundary layer (Cassiani et al., 2015). In addition to the third moment, Franzese et al. (1999) have pointed that any statistical distribution model of turbulent velocity is not needed to be predefined in the Lagrangian model if the fourth order moment is also used.

The profiles of the third-order (μ_i) and the fourth-order (ϕ_i, $i = u, v, w$) moments for lateral, transversal, and vertical turbulent velocities are shown in Fig. 4. For comparison with the Gaussian distribution, the third- and fourth-order moments are normalized by the turbulent standard deviations. For the Gaussian distribution, the normalized third-order moment (i.e., skewness) equals 0 and the normalized fourth-order moment (i.e., kurtosis) equals 3. Any variable deviating from the Gaussian distribution will have its skewness and kurtosis significantly deviating from 0 and 3 respectively. From Fig. 4, one can see that the turbulent velocity fluctuations for the horizontal components in the TS significantly deviate from the Gaussian distribution at higher heights. In contrast, the turbulent velocity fluctuations in the CS and DS approximately satisfy the Gaussian distribution. In the TS, the skewness is significantly greater than 0 and the kurtosis approximates to 3 for the lateral turbulent velocity fluctuations; the skewness approximates to 0 but the kurtosis is significantly greater than 3 for the transversal turbulent velocity fluctuations. The results indicate that in the TS the statistical distribution of the transversal velocity fluctuations is approximately symmetrical but has a long tail; the statistical distribution of the lateral turbulent velocity fluctuations is asymmetrical and skews to the left. The non-Gaussian of turbulent wind velocity fluctuations could be related to the intermittent coherent structures in the atmospheric boundary layer, such as the ejection-sweep sequences (Aubry et al., 1988; Feigenwinter and Vogt, 2005).

The local similarity relations of the third-order moments for lateral, transversal, and vertical turbulent velocities are shown in Fig. 5. As the similarity functions of turbulent standard deviations, the similarity function of the third-order moments in the TS is obviously different from those in the CS and DS. The similarity functions in the CS and DS are almost the same. The values of $|\mu_u|^{1/3}/u_l$ in the TS are generally larger than those in the CS and DS. The values of $|\mu_v|^{1/3}/u_l$ in the TS approximately equal to those in the CS and DS in nearly neutral conditions but normally increase faster in highly stable or unstable conditions. The values of $|\mu_w|^{\frac{1}{3}}/u_l$ in the three stages are nearly the same. The similarity functions of turbu-

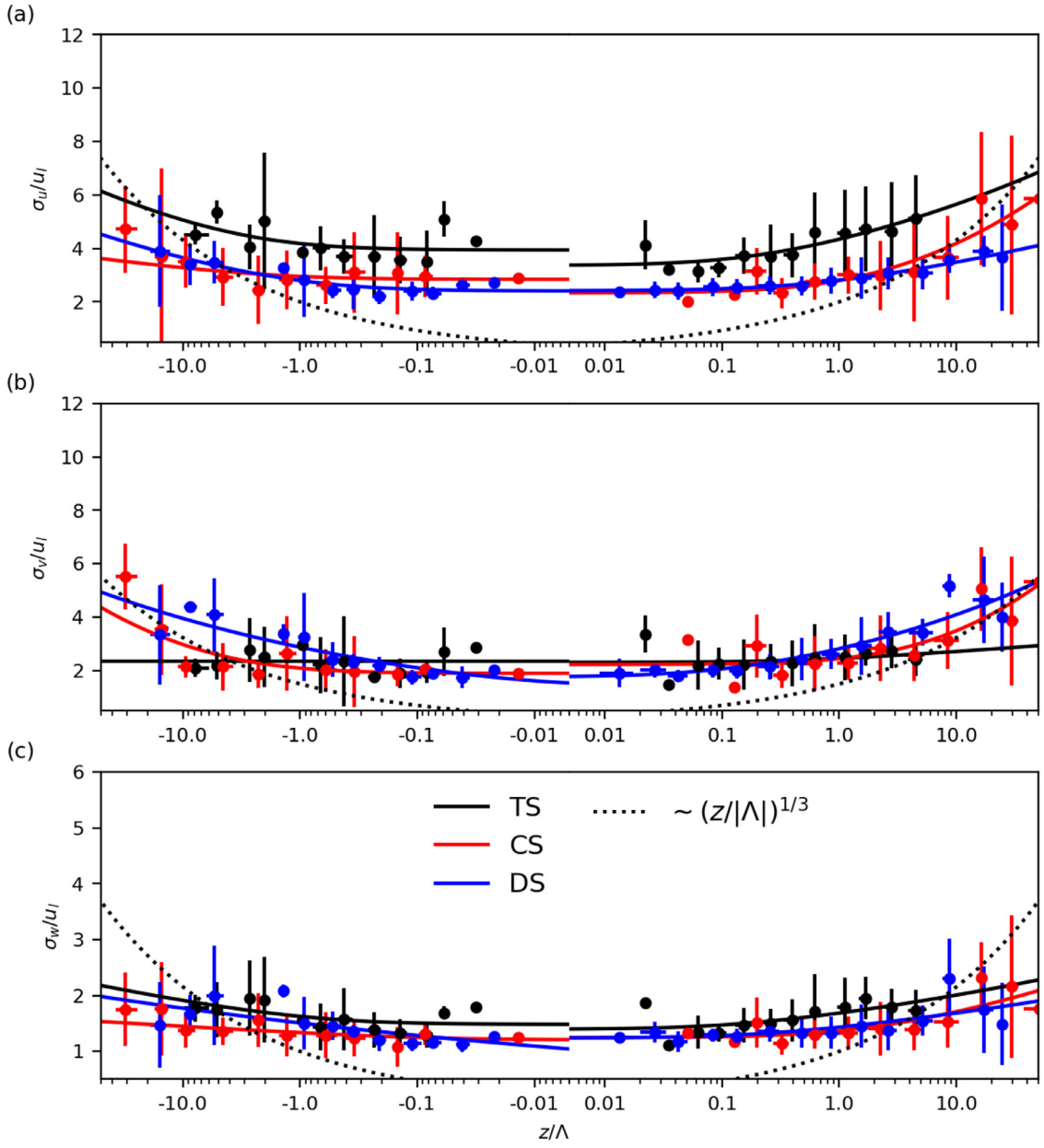

Fig. 3 – Local similarity relations of turbulent standard deviations for (a) longitudinal, (b) transversal, and (c) vertical wind velocities in the TS (black points), the CS (red points), and the DS (blue points). Data are fitted by Eq. (2). The fitting curves are shown by lines and the curves of the local free convection assumption are shown by dotted lines.

lent third-order moments can be fitted by

$$\frac{|\mu_i|^{\frac{1}{3}}}{u_l} = \left(a_i + b_i \frac{z}{\Lambda}\right)^{c_i}, \tag{3}$$

where a_i, b_i, and c_i are fitting parameters and $i = u, v, w$. The fitted values are listed in Table 2. The results also show that the turbulent third-order moments normally deviate from the assumption of free convection in the very stable or unstable conditions.

The local similarity relations of the turbulent fourth-order moments for lateral, transversal, and vertical wind velocities are shown in Fig. 6. It is found that the values of $|\phi_u|^{\frac{1}{4}}/u_l$ in the TS are significantly larger than those in the CS and DS. The nearly neutral values of $|\phi_w|^{\frac{1}{4}}/u_l$ in the TS approximately equal to those in the CS and DS, but in the highly unstable and stable conditions $|\phi_w|^{\frac{1}{4}}/u_l$ normally increase more quickly than that in the CS and DS. The similarity function of the turbulent fourth-order moments is fitted by

$$\frac{|\phi_i|^{\frac{1}{4}}}{u_l} = \left(a_i + b_i \frac{z}{\Lambda}\right)^{c_i}, \tag{4}$$

where a_i, b_i, and c_i are fitting parameters and $i = u, v, w$. The fitted parameters are listed in Table 2. The results show that the turbulent fourth-order moments also deviate from the as-

Table 1 – The nearly neutral values of dimensionless turbulent standard deviations a_i (i = u, v, w) and the free convention exponent c_i estimated by fitting data collected in unstable urban boundary layer with Eq. (2).

References	a_u	a_v	a_w	c_u	c_v	c_w
Al-Jiboori et al. (2002)	1.75	1.60	1.22	1/3	1/3	1/3
Quan et al. (2009)	2.03	1.70	1.33	1/3	1/3	1/3
Wood et al. (2010)	2.23	1.78	1.31	1/3	1/3	1/3
Pegahfar et al. (2017)	3.23	3.42	2.38	1/3	1/3	1/3
Fortuniak et al. (2013)	2.33	1.60	1.11	0.43	0.32	0.54
	2.21	1.74	1.21	0.43	0.28	0.43
Yusup et al. (2016)	—	2.51	1.41	—	0.27	0.24
	—	1.98	1.10	—	0.35	0.32
Ren et al. (2019)	2.27	2.01	1.25	1/3	1/3	1/3
	2.77	2.82	1.45	1/3	1/3	1/3

Note: The upper and lower rows in Fortuniak et al. (2013) list results obtained at two sites; the upper and lower rows inYusup et al. (2016) list results with different wind directions; the upper and lower rows in Ren et al. (2019) list results under haze and clean conditions respectively.

Table 2 – The parameters obtained by fitting data with Eqs. (2) – (4) for turbulent standard deviations and turbulent third and fourth order moments respectively.

Stability	Parameters	TS			CS			DS		
		a	b	c	a	b	c	a	b	C
$\Lambda < 0$	σ_u	3.94	0.59	0.13	2.84	0.78	0.07	2.41	1.99	0.14
	σ_v	2.35	0.00	0.00	1.89	0.46	0.26	1.41	173.08	0.14
	σ_w	1.48	2.03	0.08	1.21	15.38	0.04	0.69	7.33e+04	0.07
	μ_u	2.89	0.91	0.07	1.98	0.03	0.27	0.85	46.16	0.18
	μ_v	1.83	0.00	0.00	1.19	0.25	0.38	0.97	245.81	0.08
	μ_w	0.85	0.72	0.24	0.41	1.33e+06	0.05	0.45	6.57e+04	0.07
	ϕ_u	4.97	3.05	0.09	3.58	0.16	0.19	3.10	1.21	0.17
	ϕ_v	3.51	0.00	0.00	2.69	0.13	0.41	2.18	65.38	0.13
	ϕ_w	2.06	4.89	0.07	1.58	2.86	0.07	1.49	59.49	0.07
$\Lambda > 0$	σ_u	3.36	7.55	0.12	2.33	1.24	0.23	2.42	3.29	0.10
	σ_v	2.30	2.84	0.05	2.22	0.41	0.28	1.76	16.54	0.17
	σ_w	1.39	10.14	0.08	1.24	1.07	0.13	1.24	6.04	0.08
	μ_u	1.89	1.84e+05	0.05	1.71	1.52	0.19	1.11	76.94	0.11
	μ_v	1.63	0.00	0.00	1.57	0.10	0.47	0.94	8.28	0.21
	μ_w	0.74	4.36	0.09	0.78	0.78	0.13	0.81	0.11	0.16
	ϕ_u	4.83	3.61	0.11	3.04	1.36	0.21	3.11	2.35	0.13
	ϕ_v	3.55	0.00	0.00	2.90	0.60	0.24	2.37	19.19	0.15
	ϕ_w	2.10	4.14	0.05	1.70	0.95	0.14	1.67	8.70	0.07

sumption of free convection in the highly stable or unstable conditions, as found in the turbulent standard deviations and the third-order moments.

3. Summary

The commonly used similarity relations of turbulence dispersion in dispersion models are based on observations in highly flat and sparsely populated areas, and they would be too simple to describe turbulence dispersion under heavy haze conditions that are intimately related to human activities in urban areas with complicated terrains. In this paper, the high-frequency turbulence data, obtained by seven ultrasonic anemometers on the Beijing 325-m meteorological tower, are used to analyze turbulence dispersion parameters, including turbulent standard deviations and turbulent third and fourth order moments under heavy haze conditions in wintertime of Beijing.

The haze processes in wintertime of Beijing are normally divided into three stages: the transport stage (TS), the cumulative stage (CS), and the dispersion stage (DS). The results show that the turbulent standard deviations in the CS are almost constant with the heigh. The values of turbulent standard deviations in the CS are also smaller than those in the TS and DS. Nearly calm wind and strong temperature inversion always appears in the CS, and turbulence is strongly depressed in this stage. The maxima appear in the profiles of turbulent standard deviations in TS and DS, and the heights where the maxima appear are significantly different for the lateral velocity components in the two stages. The appearance of maxima would be related to strong wind shears over building tops and the heights where the maxima appear represent the average building heights in the dominant wind directions, as found in many wind-tunnel experiments and numerical

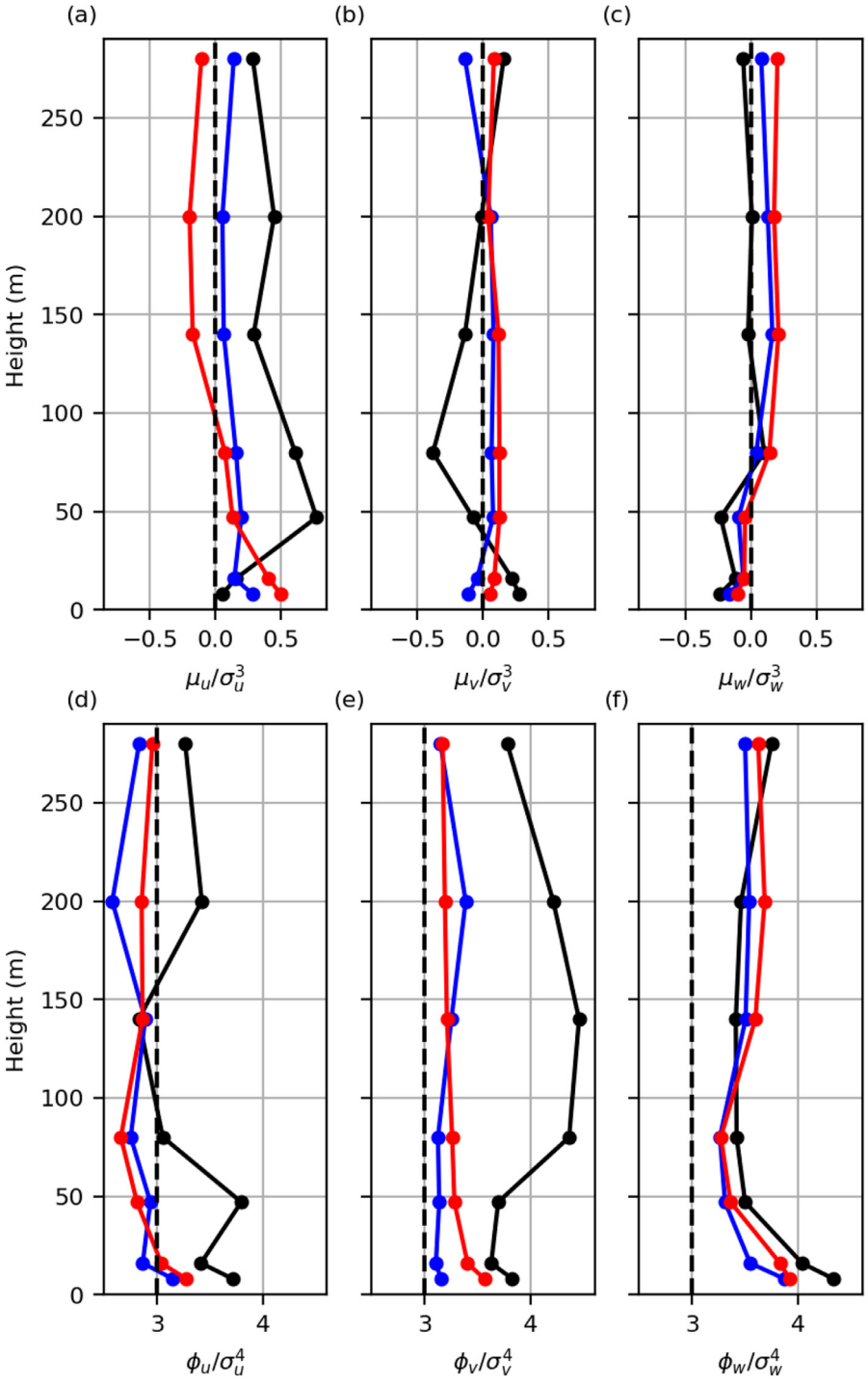

Fig. 4 – Profiles of turbulent (a-c) third-order and (d-e) fourth-order moments for longitudinal, transversal, and vertical wind velocities in the TS (black), the CS (red) and the DS (blue). The vertical dotted lines are the values of the Gaussian distribution.

simulations (Kastner-Klein and Rotach, 2004; Christen et al., 2009; Giometto et al., 2016). The analysis of skewness and kurtosis shows that turbulent wind velocities in the CS and DS approximately satisfy the Gaussian distribution, while the lateral and transversal turbulent wind velocities in the TS significantly deviate from the Gaussian distribution. Thus, the classical Gaussian dispersion models would not be suitable to simulate horizontal turbulence dispersion in the TS.

The analysis of local similarity relations shows that similarity functions in the TS are normally different from those in the CS and DS. For lateral wind velocities, the similarity functions of turbulent standard deviations in the TS are generally larger than those in the CS and DS. For vertical wind velocities, the similarity functions of turbulent standard deviations

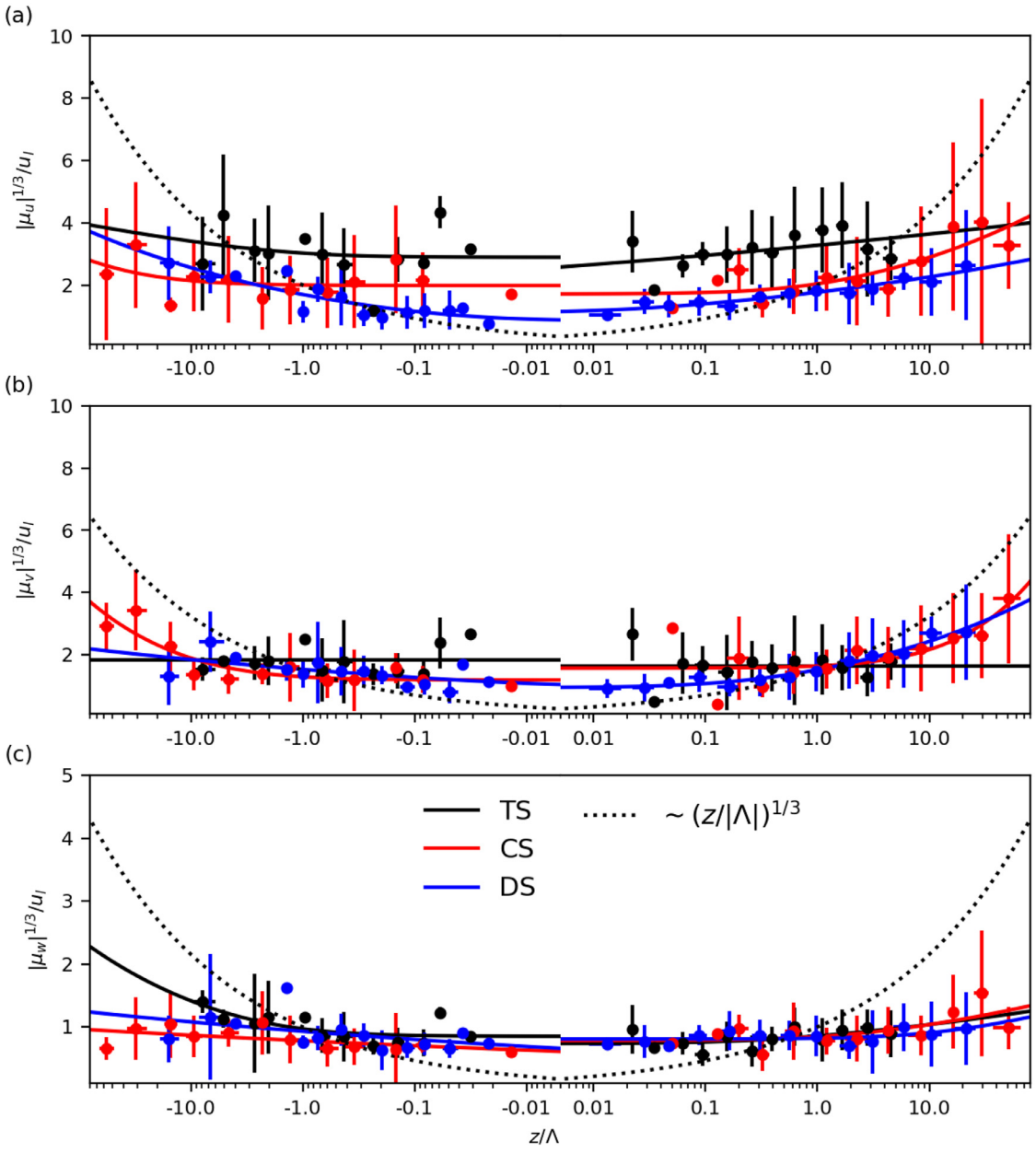

Fig. 5 – Local similarity relations of turbulent third-order moments for (a) longitudinal, (b) transversal, and (c) vertical components in the TS (black points), the CS (red points), and the DS (blue points). Data are fitted by Eq. (3). The fitting curves are shown by lines and the curves of the local free convection assumption are shown by dotted lines.

in the TS generally increase much faster than those in the CS and DS in highly stable or unstable conditions. As the turbulent standard deviations, the local similarity functions of the third and fourth order moments in the TS are also found to be different from those in the CS and DS; the former is generally larger than the latter.

This work indicates that under heavy haze conditions a single similarity relation cannot describe turbulence dispersion. The multiple similarity relations should be used in the parameterization of turbulence dispersion. Although the present study focuses on the heavy haze pollution in wintertime of Beijing, the topics can also be discussed in other places in future work. The pollutant concentration is affected by many meteorological factors, and turbulence is only one of the important factors (Zhong et al., 2017a,b; Zhang et al., 2019). In fact, many meteorological factors that affect the pollutant concentration, such as temperature inversion and radiation, would also affect turbulence. In addition, the influence of pollutants on radiation will in turn affect turbulence. The complex interaction between turbulence and pollutant concentration is worthy of attention in future work. The study of the flux-profile relationship during heavy haze processes is also an interesting topic. It could be helpful for designing the turbulence diffusion parameterization scheme in the Eu-

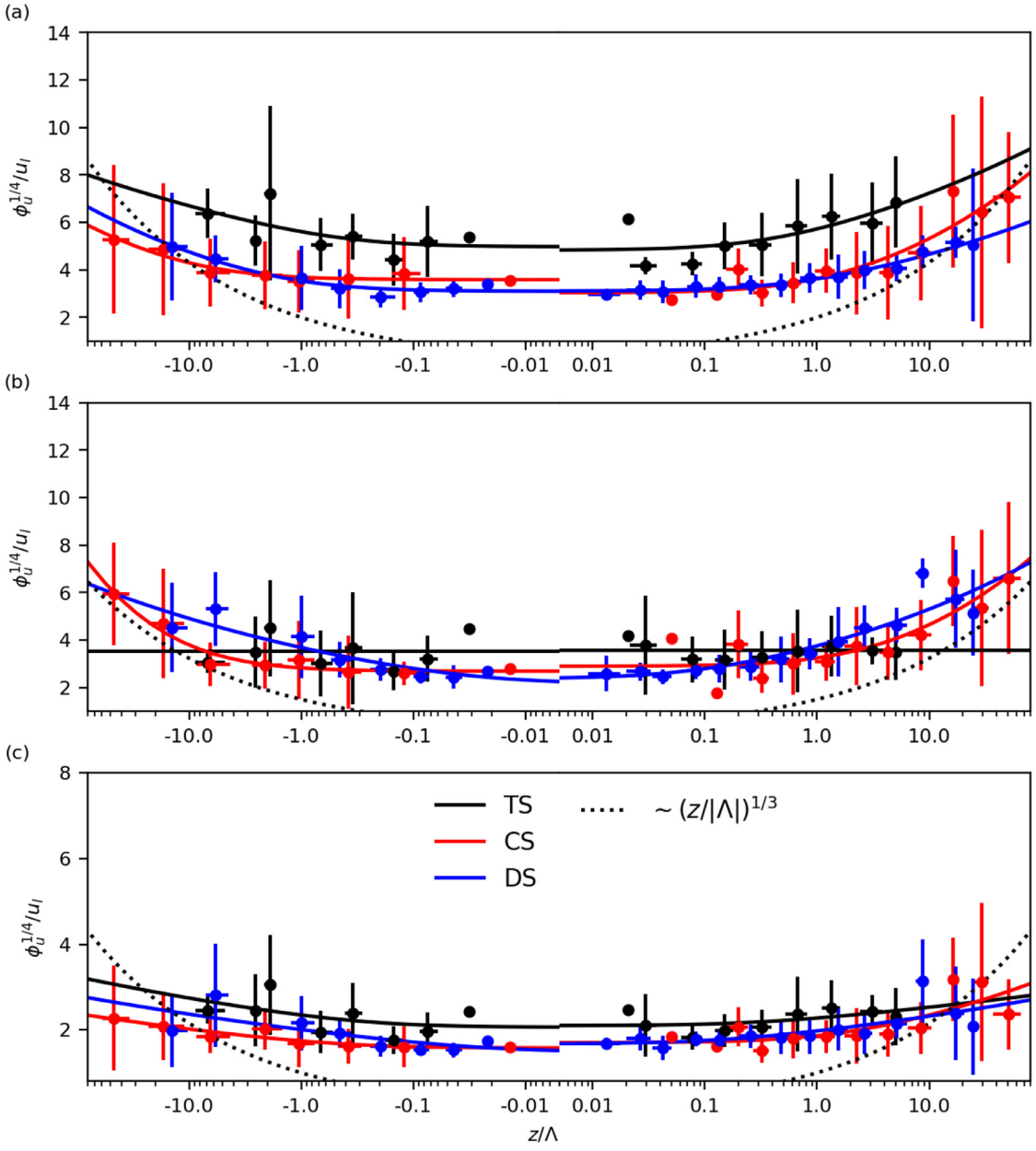

Fig. 6 – Local similarity relations of turbulent fourth-order moments for (a) longitudinal, (b) transversal, and (c) vertical wind velocities in the TS (black points), the CS (red points), and the DS (blue points). Data are fitted by Eq. (4). The fitting curves are shown by lines and the curves of the local free convection assumption are shown by dotted lines.

ler models. We hope that this topic could also be systematically studied in further work.

Acknowledgments

This work was supported by the National Natural Science Foundation of China (No. 41975018) and the General Financial Grant from the China Postdoctoral Science Foundation (No. 2020M670420).

REFERENCES

Aubry, N., Holmes, P., Lumley, J.L., Stone, E., 1988. The dynamics of coherent structures in the wall region of a turbulent boundary layer. J. Fluid Mech. 192, 115–173.

Al-Jiboori, M.H., Xu, Y., Qian, Y., 2002. Local similarity relationships in the urban boundary layer. Boundary-Layer Meteorol 102, 63–82.

Bei, N., Li, X., Tie, X., Zhao, L., Wu, J., Li, X., et al., 2020. Impact of synoptic patterns and meteorological elements on the wintertime haze in the Beijing-Tianjin-Hebei region, China from 2013 to 2017. Sci. Total Environ. 704, 135210.

Christen, A., Rotach, M.W., Vogt, R., 2009. The budget of turbulent kinetic energy in the urban roughness sublayer. Boundary-Layer Meteorol 131, 193–222.
Cassiani, M., Stohl, A., Brioude, J., 2015. Lagrangian stochastic modelling of dispersion in the convective boundary layer with skewed turbulence conditions and a vertical density gradient: Formulation and implementation in the FLEXPART model. Boundary-Layer Meteorol 154, 367–390.
Du, H., Li, J., Chen, X., Wang, Z., Sun, Y., Fu, P., et al., 2019. Modeling of aerosol property evolution during winter haze episodes over a megacity cluster in northern China: roles of regional transport and heterogeneous reactions of SO2. Atmos. Chem. Phys. 19, 93519370.
Fortuniak, K., Pawlak, W., Siedlecki, M., 2013. Integral turbulence statistics over a central European city centre. Boundary-Layer Meteorol 146, 257–276.
Franzese, P., Luhar, A.K., Borgas, M.S., 1999. An efficient Lagrangian stochastic model of vertical dispersion in the convective boundary layer. Atmos. Environ. 33, 2337–2345.
Feigenwinter, C., Vogt, R., 2005. Detection and analysis of coherent structures in urban turbulence. Theor. Appl. Climatol. 81, 219–230.
Giometto, M.G., Christen, A., Meneveau, C., 2016. Spatial characteristics of roughness sublayer mean flow and turbulence over a realistic urban surface. Boundary-Layer Meteorol 160, 425–452.
Guo, L., Chen, B., Zhang, H., Zhang, Y., 2020. A new approach combining a simplified FLEXPART model and a Bayesian-RAT method for forecasting PM10 and PM2.5. Environ. Sci. Pollut. Res. 27, 2165–2183.
Garratt, J. R., 1992: The Atmospheric Boundary Layer. Cambridge University Press, 331pp
Hong, Q., Liu, C., Hu, Q., Xing, C., Tan, W., Liu, T., et al., 2021. Vertical distributions of tropospheric SO2 based on MAX-DOAS observations: Investigating the impacts of regional transport at different heights in the boundary layer. J. Environ. Sci. 103, 119–134.
Kaimal, J. C., and J. J. Finnigan, 1994: Atmospheric Boundary Layer Flows: Their Structure and Measurement. Oxford University Press, 289 pp.
Kastner-Klein, P., Rotach, M.W., 2004. Mean flow and turbulence characteristics in an urban roughness sublayer. Boundary-Layer Meteorol 111, 55–84.
Luhar, A.K., Hibberd, M.F., Borgas, M.S., 2000. A skewed meandering plume model for concentration statistics in the convective boundary layer. Atmos. Environ. 34, 3599–3616.
Li, J., Sun, J., Zhou, M., Cheng, Z., Li, Q., Cao, X., et al., 2017. Observational analyses of dramatic developments of a severe air pollution event in the Beijing area. Atmos. Chem. Phys. 18, 3919–3935.
Liu, L., Shi, Y., Hu, F., 2021. Characteristics and similarity relations of turbulence dispersion parameters under heavy haze conditions. Atmos. Pollut. Res. 12, 330–340.
Miao, Y.C., Liu, S.H., Zheng, Y.J., Wang, S., Liu, Z.X., Zhang, B., 2015. Numerical study of the effects of Planetary Boundary Layer structure on the pollutant dispersion within built-up areas. J. Environ. Sci. 32, 168–179.
Panofsky, H.A., Tennekes, H., Lenschow, D.H., Wyngaard, J.C., 1977. The characteristics of turbulent velocity components in the surface layer under convective conditions. Boundary-Layer Meteorol 11, 355–361.
Pegahfar, N., Zawarreza, P., 2017. Observed turbulence characteristics in unstable conditions over the city of Tehran based on similarity theory. Meteor. Atmos. Phys. 129, 479–494.
Quan, L., Hu, F., 2009. Relationship between turbulent flux and variance in the urban canopy. Meteorol. Atmos. Phys. 104, 29–36.
Ren, Y., Zhang, H., Wei, W., Wu, B., Liu, J., Cai, X., et al., 2019. Comparison of the turbulence structure during light and heavy haze pollution episodes. Atmos. Res. 230, 104645.
Stohl, A., Forster, C., Frank, A., Seibert, P., Wotawa, G., 2005. Technical note: The Lagrangian particle dispersion model FLEXPART version 6.2. Atmos. Chem. Phys. Discuss. 5, 4739–4799.
Roth, M., 2000. Review of atmospheric turbulence over cities. Q. J. R. Meteorol. Soc. 126, 941–990.
Salmond, J.A., McKendry, I.G., 2005. A review of turbulence in the very stable nocturnal boundary layer and its implications for air quality. Prog. Phys. Geog. 29, 171–188.
Shi, Y., Hu, F., 2020. Ramp-Like PM Accumulation Process and Z-Less Similarity in the Stable Boundary Layer. Geophys. Res. Lett. 47, e2019GL086530.
Stull, R. B., 1988. An introduction to boundary layer meteorology. Kluwer Academic Publishers, Dordrecht.
Thomson, D.J., 1987. Criteria for the selection of stochastic models of particle trajectories in turbulent flows. J. Fluid Mech. 180, 529–556.
Vickers, D., Mahrt, L., 1997. Quality control and flux sampling problems for tower and aircraft data. J. Atmos. Ocean Tech. 14, 512–526.
Wood, C.R., Lacser, A., Barlow, J.F., Padhra, A., Belcher, S.E., Nemitz, E., et al., 2010. Turbulent flow at 190m height above London during 2006-2008: A climatology and the applicability of similarity theory. Boundary-Layer Meteorol 137, 77–96.
Wang, L., Liu, J., Gao, Z., Li, Y., Huang, M., Fan, S., et al., 2019. Vertical observations of the atmospheric boundary layer structure over Beijing urban area during air pollution episodes. Atmos. Chem. Phys. 19, 6949–6967.
Yusup, Y., Anis, S.I., 2016. Similarity theory and nocturnal locally scaled turbulence variances in the tropical urban roughness sublayer. In: Atmospheric Pollution Research, 7, pp. 454–468.
Zhong, J., Zhang, X., Dong, Y., Wang, Y., Liu, C., Wang, J., et al., 2017a. Feedback effects of boundary-layer meteorological factors on cumulative explosive growth of PM 2.5 during winter heavy pollution episodes in Beijing from 2013 to 2016. Atmos. Chem. Phys. 18, 247–258.
Zhong, J.T., Zhang, X, Wang, Y, Sun, J., Zhang, Y., Wang, J., et al., 2017b. Relative contributions of boundary-layer meteorological factors to the explosive growth of PM2.5 during the red-alert heavy pollution episodes in Beijing in December 2016. J. Meteor. Res. 31, 809–819.
Zhang, X., Xu, X., Ding, Y., Liu, Y., Zhang, H., Wang, Y., et al., 2019. The impact of meteorological changes from 2013 to 2017 on PM 2.5 mass reduction in key regions in China. Sci. China Earth Sci. 62, 1885–1902.